ISSN: 2641-2039
DOI: 10.33552/GJES.2022.09.000711
Global Journal of Engineering Sciences
Iris Publishers

Research Article

Analytical Modeling of Transient Heat Transfer Coupled with Fluid Flow in Subsurface Thermal Recovery Process: Heat Transfer Coupled with Steady Flow

Kuizheng Yu, Wanju Yuan, Min Yang and Gang Zhao*

Petroleum Systems Engineering, Faculty of Engineering and Applied Science, University of Regina, Wascana Parkway, Regina, Saskatchewan, Canada

***Corresponding author:** Gang Zhao, Petroleum Systems Engineering, Faculty of Engineering and Applied Science, University of Regina, 3737 Wascana Parkway, Regina, Saskatchewan S4S 0A2, Canada.

Received Date: February 22, 2022

Published Date: March 07, 2022

Abstract

Thermal recovery methods based on steam injection have become the most successful techniques for subsurface heavy oil and bitumen reservoirs in western Canada. It is commonly suggested that heat conduction is the dominant mechanism of heat transfer near the edge of steam chamber. Heat convection is neglected in classical models, such as in Butler's theory. Recently, it has been realized that heat convection also plays a significant role in heat transfer during thermal recovery process. In this study, a novel analytical model integrating heat conduction and heat convection is developed to describe the transient heat transfer coupled with steady flow in thermal recovery process. In steady flow, subsurface reservoir and fluid properties are integrated into two newly defined constant parameters, i.e., thermal diffusivity of subsurface reservoir and fluid system, and thermal convection velocity of injection fluid. Various cases representing different steam injection strategies are studied. The analytical solution of each case is derived and validated with numerical simulations. Subsequently, the effects of thermal diffusivity and thermal convection velocity are examined. It is found that convective and conductive heat transfer occur simultaneously during thermal recovery process. Heat convection accounts for a much higher percentage of the total heat transferred than heat conduction. Fluid flow motivates heat convection and greatly increases the rate of heat transfer. It is also found that the temperature curves of analytical solutions are consistent with the numerical simulation results. The newly developed mathematical models and analytical solutions are simple and efficient to obtain the temperature profiles in thermal recovery and geothermal reservoir production process.

Keywords: Analytical modeling; Heat transfer; Steady flow; Thermal recovery; Subsurface reservoirs; Heavy oil; Geothermal reservoir; Energy production

Nomenclature: c - specific heat capacity ($J \cdot kg^{-1} \cdot K^{-1}$); cρ - volumetric heat capacity ($J \cdot m^{-3} \cdot K^{-1}$); d – conduction; D - thermal diffusivity (m^2/s); erfc - complementary error function; f – fluid; i - initial condition; k - permeability (μm^2); K - thermal conductivity ($W \cdot m^{-1} \cdot K^{-1}$); l – liquid; L^{-1} - inverse Laplace transformation; o – oil; P - pressure (Pa); q_d - conductive heat flux (W/m^2); q_v - convective heat flux (W/m^2); q_w - surface water rate of injector (m^3/day); q_l - surface liquid rate of producer (m^3/day); Q - rate of heat generation per unit volume (W/m^3); r – reservoir; s_{oi} - initial oil saturation; T - temperature (K); T_D - dimensionless temperature; t - time (s); t_D - dimensionless time; u - thermal convection velocity (m/s); v – convection; V - darcy's velocity (m/s); w – water; x - distance (m); x_D - dimensionless distance; CMG - Computer Modelling Group; CSS - Cyclic Steam Stimulation; ISC - In-Situ Combustion; SAGD - Steam-Assisted Gravity Drainage; STARS - Steam, Thermal and Advanced processes Reservoir Simulator

Greek letters: ϕ – porosity; ρ - density (kg/m^3); μ - viscosity (Pa·s); λ - flow resistance coefficient (s^{-1}); β - exponential decay coefficient (m^{-1}); ω - Coefficient defined in Equation (18) (m/s)

Introduction

Western Canada holds tremendous subsurface reservoirs, including geothermal and heavy oil resources, for heavy oil alone with an estimated original oil in place of 5.7 billion m^3 in Alberta and 3.4 billion m^3 in Saskatchewan, respectively [1]. Three largest heavy oil and bitumen deposits in Alberta are Athabasca Wabiskwa-McMurray, Cold Lake Clearwater and Peace River Bluesky-Gething [2]. In Saskatchewan, heavy oil and bitumen deposits are found in the Bakken formation and the Mannville group [3]. The geographical distributions of heavy oil and bitumen deposits in western Canada are shown in Figure 1.

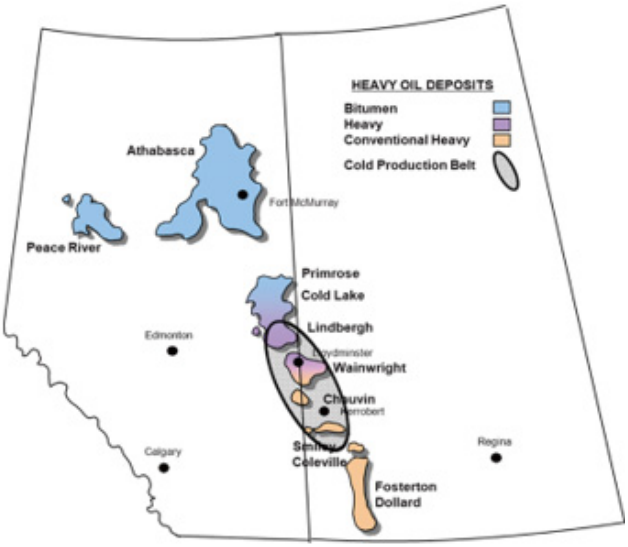

Figure 1: Subsurface heavy oil deposits in western Canada (Courtesy of Alberta Department of Energy).

The key to heavy oil recovery is to reduce oil viscosity and hence improve the oil mobility. Thermal recovery methods, using heat to reduce oil viscosity in-situ, have been most successful, and currently account for the production of over one-half million barrels of oil per day in the U.S., Venezuela, and Canada [4]. At present, the most commonly used thermal recovery techniques in western Canada are steam-assisted gravity drainage (SAGD) [5], cyclic steam stimulation (CSS) [6], in-situ combustion (ISC) [7], steam flooding and hot water flooding. Thermal recovery methods are effective as oil viscosity is very sensitive to temperature. Increasing the temperature of oil in the subsurface reservoir leads to the reduction of oil viscosity by several orders of magnitude. Figure 2 displays the viscosity profile versus temperature of Athabasca bitumen [8].

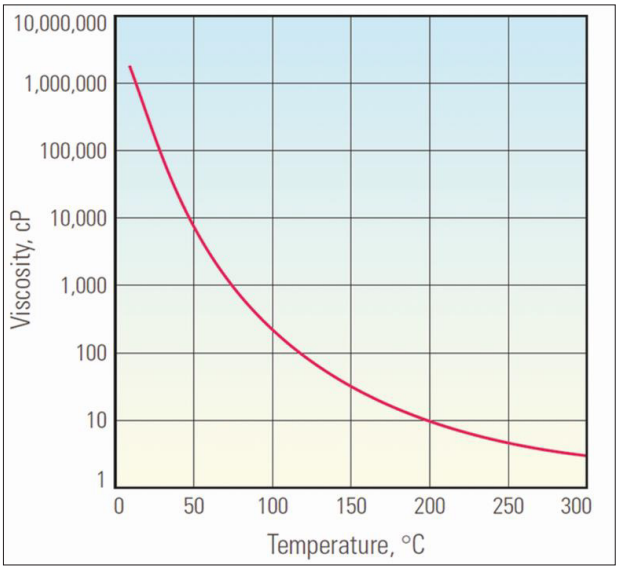

Figure 2: Effect of temperature on viscosity of Athabasca bitumen [8].

Therefore, it is of fundamental and practical importance to mathematically model heat transfer during thermal recovery process in order to better understand the steam chamber development and oil production mechanisms. It is traditionally suggested that heat conduction is the dominant mechanism of heat transfer near the edge of steam chamber. Heat convection is neglected in classical models, such as in Butler's theory [9]. Recently, it has been widely realized that convective heat transfer also plays a significant role in heat transfer at the edge of steam chamber.

Theory of Heat Transfer Coupled with Fluid Flow

Conductive and convective heat transfer

Conductive heat transfer occurs at the molecular scale by means of collisions and interactions between molecules at different energy states, namely conductive heat transfer is caused by temperature difference between adjacent particles. When hot fluid is injected into subsurface reservoir, its heat is transferred to the molecules it contacts, which in turn, conduct heat to neighboring molecules and so on [10, 11], The Fourier's equation below shows the conductive heat flux [12, 13]:

$$\overrightarrow{q_d} = -K\nabla T \tag{1}$$

where $\overrightarrow{q_d}$ is conductive heat flux, K is thermal conductivity, ∇T is temperature gradient.

Convective heat transfer occurs when hot fluid flows within the subsurface reservoir, and heat is transferred through the movements of particles within the hot fluid to heat the volumes occupied by the hot fluid [10, 11]. The velocity of fluid flow can be calculated using Darcy's law. The following equations show the convective heat flux and Darcy's velocity [12, 13]:

$$\overrightarrow{q_v} = \rho_f c_f \vec{V}(T - T_r) \tag{2}$$

$$\vec{V} = -\frac{k}{\mu}\nabla P \tag{3}$$

where $\overrightarrow{q_v}$ is convective heat flux, ρ_f is fluid density, c_f is specific heat capacity of injection fluid, $\vec{v}$ is Darcy's velocity, k is subsurface reservoir permeability, μ is fluid viscosity, P is pressure, T is the temperature of injection fluid, and T_r is initial subsurface reservoir temperature.

During every convective heat transfer process, conductive heat transfer occurs as well at the same time. Conductive and convective heat transfer occur simultaneously in porous media with fluid flow. This process is shown in Figure 3 [10]. Heat conduction is caused by temperature gradient, while heat convection is caused by fluid flow that motivated by pressure gradient. The stationary fluids and subsurface reservoir matrix are heated by heat conduction, while the displacement of oil and movement of injection fluid in subsurface reservoir are the sources of heat convection. Convective heat transfer transports the energy of a moving heat source to further distance along the direction of fluid flow, while conductive heat transfer conducts heat to the surroundings in all directions at the same time [10, 11].

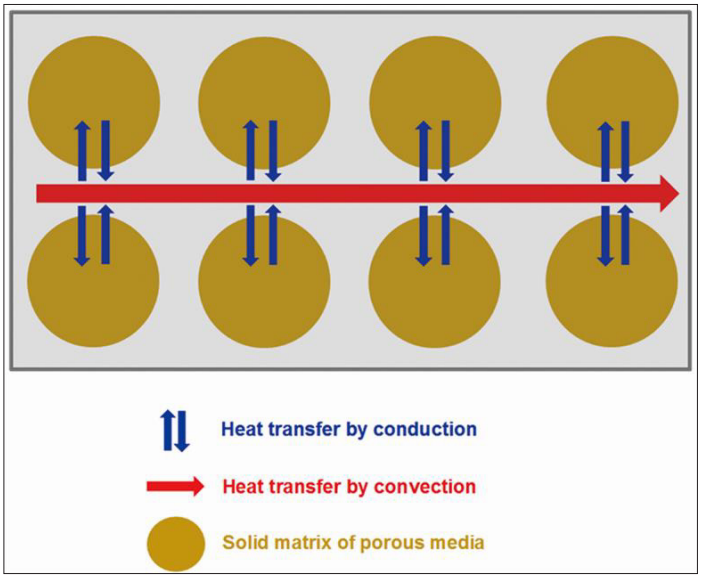

Figure 3: Heat transfer mechanisms in molecules of porous media [10].

Equation of heat transfer coupled with fluid flow

The equation of transient heat transfer can be constructed by performing an energy balance on a small control volume. The following partial differential equation combining conductive heat flux and convective heat flux is then derived to describe the heat transfer coupled with fluid flow [10, 11]:

$$\nabla\cdot(K\nabla T) - \nabla\cdot\left(\rho_f c_f \vec{V}(T - T_r)\right) + Q = \rho c\frac{\partial T}{\partial t} \tag{4}$$

where Q is the rate of heat generation per unit volume, ρc is the overall volumetric heat capacity of subsurface reservoir and fluid system.

Assuming that the density and specific heat capacity of fluid and subsurface reservoir are constants, and the subsurface reservoir is homogeneous with a spatially constant value of thermal conductivity. And neglecting internal heat generation, i.e., Q=0. Equation (4) can be simplified and rearranged as:

$$\frac{\partial T}{\partial t}=\frac{K}{\rho c}\nabla^2 T-\frac{\rho_f c_f}{\rho c}\vec{V}\nabla T \tag{5}$$

Here, two important parameters [10, 11] are newly defined, i.e., thermal diffusivity of the subsurface reservoir and fluid system, and thermal convection velocity of injection fluid:

$$D=\frac{K}{\rho c} \tag{6}$$

$$\vec{u}=\frac{\rho_f c_f}{\rho c}\vec{V} \tag{7}$$

Substitution of Equations (6) and (7) into Equation (5) yields

$$\frac{\partial T}{\partial t}=D\nabla^2 T-\vec{u}\nabla T \tag{8}$$

The above equation is a typical convection-diffusion equation, which is the governing partial differential equation of transient heat transfer coupled with fluid flow in porous medium.

Mathematical Models and Solutions

One-dimensional heat transfer model coupled with steady flow

Under steady flow condition, the pressure gradient between the injection fluid zone and the crude oil zone is constant, which determines that the thermal convection velocity of injection fluid is constant in steady flow. The thermal diffusivity of the subsurface reservoir and fluid system is also constant [10, 11].

The partial differential equation that describes one-dimensional transient heat transfer coupled with steady flow is given by:

$$\frac{\partial T}{\partial t}=D\frac{\partial^2 T}{\partial x^2}-u\frac{\partial T}{\partial x} \tag{9}$$

where thermal diffusivity and thermal convection velocity are constant coefficients.

The general initial condition can be defined as:

$$T(x,0)=F(x),\quad x\geq 0 \tag{10}$$

As to the upper boundary condition at x=0, two different general boundary conditions are applied in the new models:

1) Temperature boundary condition [14]:

$$T(0,t)=G(t),\quad t\geq 0 \tag{11}$$

2) Heat flux boundary condition [14]:

$$-D\frac{\partial T}{\partial x}+uT=uG(t),\quad t\geq 0 \tag{12}$$

The lower boundary at x=∞ is defined as zero heat flow boundary [10, 11]:

$$\left.\frac{\partial T}{\partial x}\right|_{x\to\infty}=0,\quad t\geq 0 \tag{13}$$

Analytical solution

The objective is to characterize the temperature as a function of location and time. Figure 4 shows the flowchart of analytical solution procedure for the one-dimensional transient heat transfer models coupled with steady flow.

For convenience, mathematical model is reduced to the dimensionless form by introducing the dimensionless variables. A suitable variable transformation is used to simplify the convection-diffusion equation. Laplace transformation is performed to derive the dimensionless analytical solution in Laplace domain. Then, the analytical solution in Laplace domain can be easily converted to dimensionless analytical solution in real time domain using the table of Laplace transformations. Finally, substitutions of the variable transformation and dimensionless variables into the dimensionless solution, the final analytical solution of heat transfer model is obtained [10, 14]. The detailed derivation process of analytical solutions can be referred in Yu's master thesis [10].

Model validation

COMSOL simulation: COMSOL Multiphysics models and simulates coupled or Multiphysics phenomena based on the finite element method, which is commonly used in solving engineering problems. It has the physics-based and equation-based modeling interfaces, and the automatic and semi-automatic meshing tools.

Numerical simulations by COMSOL Multiphysics are used to validate the analytical solutions. A two-dimensional simulation model is developed to simulate the one-dimensional transient heat transfer process. Figure 5 displays the configuration of the COMSOL simulation model. The length of the model in x-direction is much larger than that in y-direction.

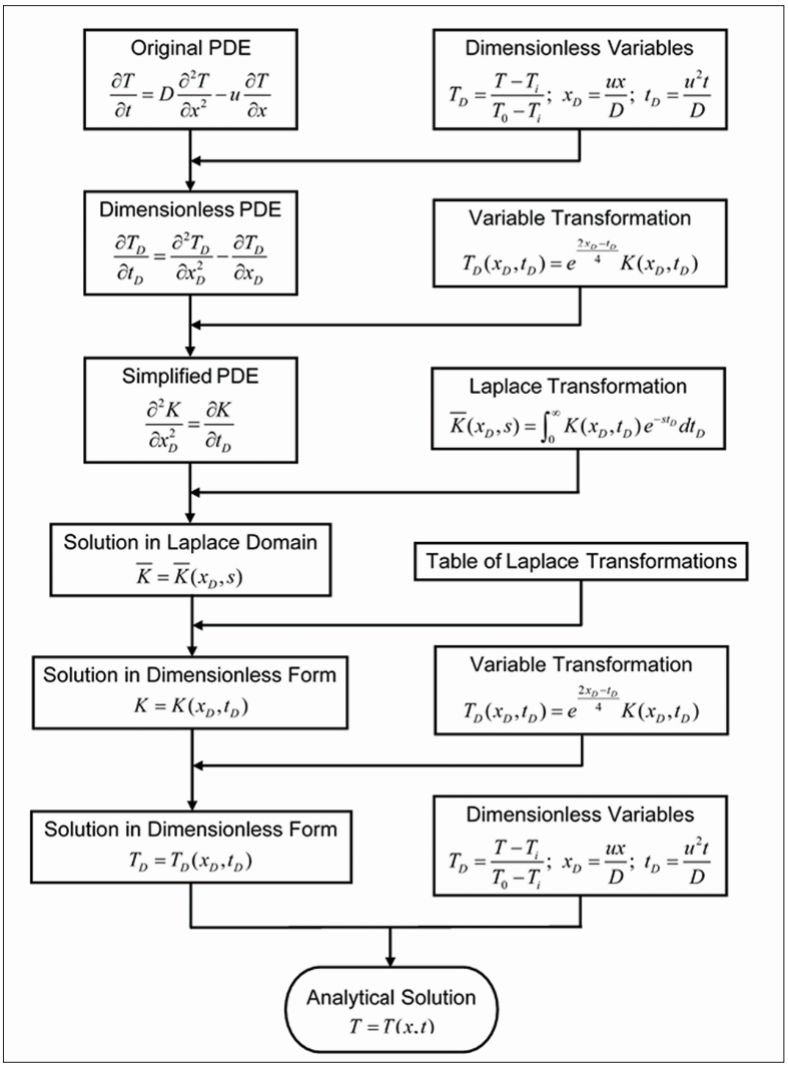

Figure 4: The flowchart of analytical solution procedure.

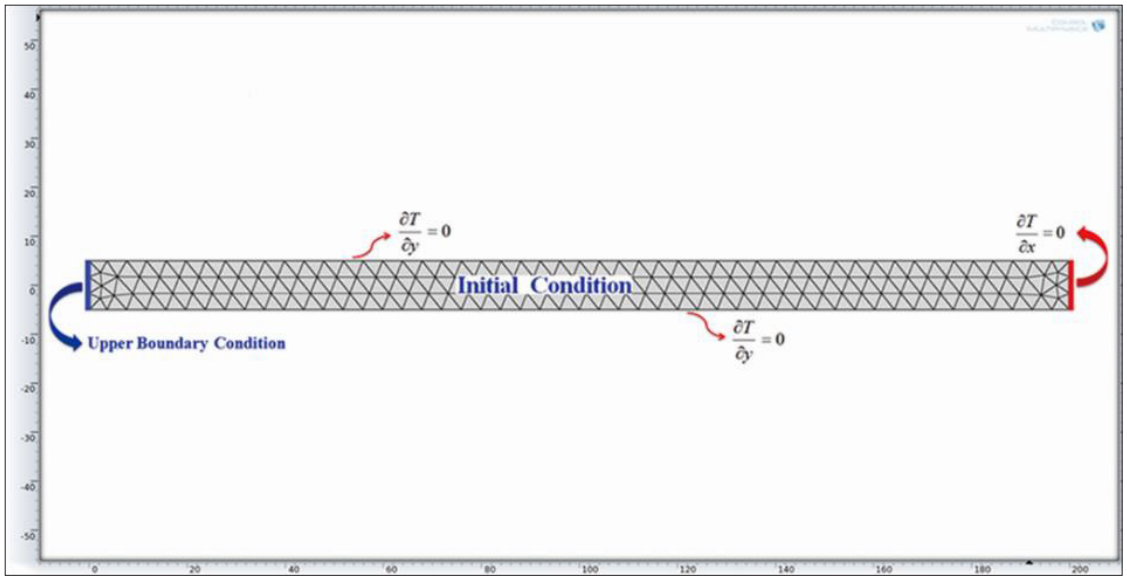

Figure 5: Configuration of the simulation model used in COMSOL Multiphysics.

CMG simulation: STARS (Steam, Thermal and Advanced processes Reservoir Simulator) developed by Computer Modelling Group Ltd. (CMG), is the leading thermal and advanced processes reservoir simulator in the oil and gas industry. STARS is ideally suitable for modeling of the complex recovery processes involving the injection of steam, solvents, air and chemicals.

The transient heat transfer in SAGD process can be described using the mathematical model in case A-1. The comparison between the analytical solution of case A-1 and CMG simulation of SAGD process is conducted. The numerical simulation model was built in a three-dimensional Cartesian coordinate system by using CMG STARS simulator, which contains 75 grids in x-direction, 4 grids in y-direction, and 25 grids in z-direction. The cell dimension is 2×100×1 m^3. The vertical distance between the horizontal injector and horizontal producer is 5 meters. The 3-D view and X-Z view of the SAGD simulation model and grid system are displayed in Figure 6. The basic parameters used in the SAGD simulation are listed in Table 1.

Table 1: Basic parameters used in the SAGD simulation model.

Parameter	Value	Unit
Initial reservoir temperature, T_i	12	°C
Initial reservoir pressure, P_i	3100	kPa
Porosity, ϕ	0.32	fraction
Permeability, k	2500	mD
Initial oil saturation, s_{oi}	0.7	fraction
Oil viscosity at reservoir temperature, μ_{oi}	11200	cp
Oil viscosity at steam temperature, μ_o	1.2	cp
Thermal conductivity of reservoir rock, K_s	6.60×10^5	J/(m·day·°C)
Thermal conductivity of oil, K_o	3.60×10^4	J/(m·day·°C)
Thermal conductivity of water, K_w	5.35×10^4	J/(m·day·°C)
Volumetric heat capacity of reservoir rock, $\rho_s c_s$	2.35×10^6	J/(m3·°C)
Specific heat capacity of oil, c_o	1675	J/(kg·°C)
Density of oil, ρ_o	980	kg/m^3
Specific heat capacity of water, c_w	4184	J/(kg·°C)
Density of water, ρ_w	1000	kg/m^3
Specific heat capacity of steam, c_{st}	4157	J/(kg·°C)
Density of steam, ρ_{st}	19.98	kg/m^3
Steam temperature, T_0	250	°C
Maximum bottom hole pressure of injector, P_0	4000	kPa
Maximum surface water rate of injector, q_w	300	m^3/day
Minimum bottom hole pressure of producer, P_1	3000	kPa
Minimum surface liquid rate of producer, q_l	600	m^3/day

Case studies

Under steady flow condition, ten cases with different initial and boundary conditions are studied. In cases A-1 to A-3, the initial subsurface reservoir temperatures are constants, and the upper boundary conditions are temperature type. In cases B-1 to B-3, the initial subsurface reservoir temperatures are constants, and the upper boundary conditions are heat-flux type. In cases C-1 to D-2, the initial subsurface reservoir temperatures are all exponentially decreasing with distance, and the upper boundary conditions are temperature type in cases C-1 and C-2, while the upper boundary conditions are heat flux type in cases D-1 and D-2. The basic parameters used in mathematical and COMSOL simulation models are listed in Table 2.

Table 2: Basic parameters used in the mathematical and COMSOL models.

Parameter	Value	Unit
Thermal diffusivity, D	0.075	m^2/day
Thermal convection velocity, u	5	cm/day
Initial reservoir temperature, T_i	12	°C
High fluid temperature, T_0	250	°C

Low fluid temperature, T_z	150	°C
Temperature increment, T_1	50	°C
Temperature increment, T_2	30	°C
Temperature changing time, t_0	2	year
Flow resistance coefficient, λ	2.5×10^{-8}	s^{-1}
Exponential decay coefficient, β	3.0×10^{-2}	m^{-1}

Case A-1

a. Mathematical model:

$$\begin{cases} \dfrac{\partial T}{\partial t} = D\dfrac{\partial^2 T}{\partial x^2} - u\dfrac{\partial T}{\partial x} \\ T(x,0) = T_i, \quad x \geq 0 \\ T(0,t) = T_0, \quad t \geq 0 \\ \left.\dfrac{\partial T}{\partial x}\right|_{x\to\infty} = 0, \quad t \geq 0 \end{cases} \tag{14}$$

b. Analytical solution:

$$T(x,t) = T_i + \frac{T_0 - T_i}{2}\left[erfc\left(\frac{x-ut}{2\sqrt{Dt}}\right) + e^{\frac{ux}{D}}erfc\left(\frac{x+ut}{2\sqrt{Dt}}\right)\right] \tag{15}$$

Case A-1 describes the continuous fluid injection at constant temperature. The temperature profiles of case A-1 predicted by both analytical solution and COMSOL are illustrated in Figure 7.

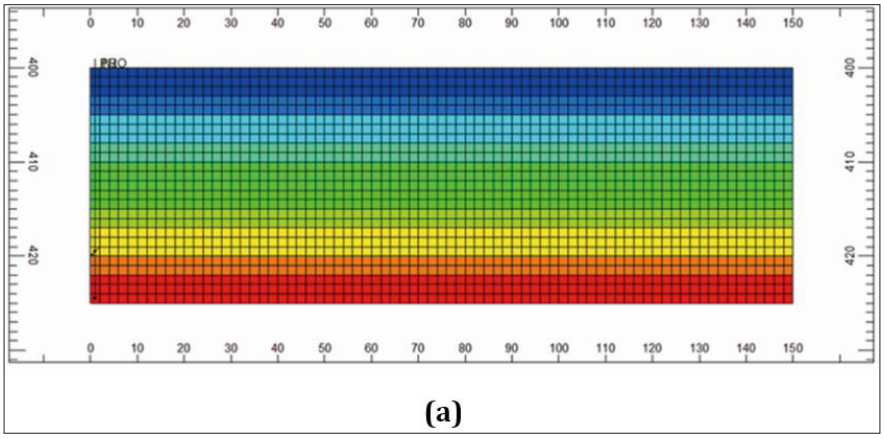

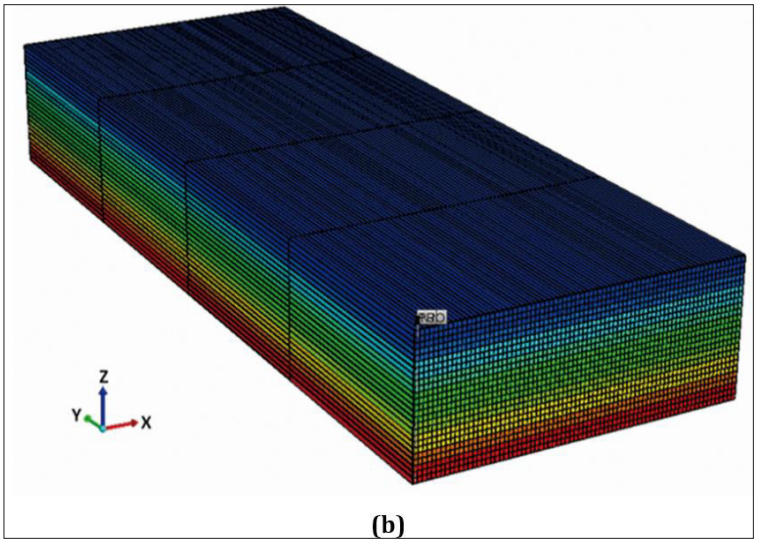

Figure 6: (a) X-Z view of the SAGD simulation model; (b) 3-D view of the SAGD simulation model.

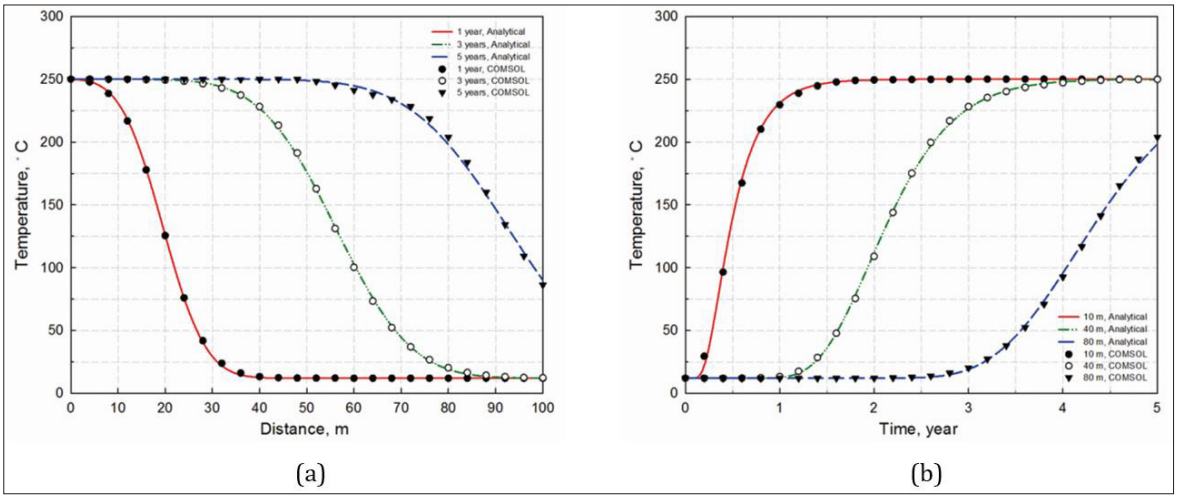

Figure 7: (a) Analytical and numerical temperature distribution as a function of distance from the injection well for case A-1 after 1 year, 3 years, and 5 years of injection; (b) Analytical and numerical temperature propagation as a function of time for case A-1 at the distance of 10 meters, 40 meters, and 80 meters from the injection well.

Case A-2:

a. Mathematical model:

$$\begin{cases} \dfrac{\partial T}{\partial t} = D\dfrac{\partial^2 T}{\partial x^2} - u\dfrac{\partial T}{\partial x} \\ T(x,0) = T_i, \quad x \geq 0 \\ T(0,t) = T_0 + T_1 e^{-\lambda t}, \quad t \geq 0 \\ \left.\dfrac{\partial T}{\partial x}\right|_{x\to\infty} = 0, \quad t \geq 0 \end{cases} \tag{16}$$

b. Analytical solution:

$$T(x,t) = T_i + \frac{1}{2}(T_0 - T_i)\left[erfc\left(\frac{x-ut}{2\sqrt{Dt}}\right) + e^{\frac{ux}{D}} erfc\left(\frac{x+ut}{2\sqrt{Dt}}\right)\right] + \frac{1}{2}T_1 e^{-\lambda t}\left[e^{\frac{(u-\omega)x}{2D}} erfc\left(\frac{x-\omega t}{2\sqrt{Dt}}\right) + e^{\frac{(u+\omega)x}{2D}} erfc\left(\frac{x+\omega t}{2\sqrt{Dt}}\right)\right] \tag{17}$$

where

$$\omega = \sqrt{u^2 - 4\lambda D} \tag{18}$$

Case A-2 describes the continuous fluid injection with exponentially decreasing temperature. The temperature profiles of case A-2 predicted by both analytical solution and COMSOL are illustrated in Figure 8.

Case A-3:

a. Mathematical model:

$$\begin{cases} \dfrac{\partial T}{\partial t} = D\dfrac{\partial^2 T}{\partial x^2} - u\dfrac{\partial T}{\partial x} \\ T(x,0) = T_i, \quad x \geq 0 \\ T(0,t) = \begin{cases} T_0, & t \leq t_0 \\ T_z, & t > t_0 \end{cases} \\ \left.\dfrac{\partial T}{\partial x}\right|_{x\to\infty} = 0, \quad t \geq 0 \end{cases} \tag{19}$$

b. Analytical solution:

$$T(x,t) = \begin{cases} T_i + \dfrac{T_0 - T_i}{2}\left[erfc\left(\dfrac{x-ut}{2\sqrt{Dt}}\right) + e^{\frac{ux}{D}} erfc\left(\dfrac{x+ut}{2\sqrt{Dt}}\right)\right], & t \leq t_0 \\ T_i + \dfrac{T_0 - T_i}{2}\left[erfc\left(\dfrac{x-ut}{2\sqrt{Dt}}\right) + e^{\frac{ux}{D}} erfc\left(\dfrac{x+ut}{2\sqrt{Dt}}\right)\right] + \dfrac{1}{2}(T_z - T_0)\, erfc\left(\dfrac{x-u(t-t_0)}{2\sqrt{D(t-t_0)}}\right) + \dfrac{1}{2}(T_z - T_0)\, e^{\frac{ux}{D}} erfc\left(\dfrac{x+u(t-t_0)}{2\sqrt{D(t-t_0)}}\right), & t > t_0 \end{cases} \tag{20}$$

Case A-3 describes the periodic fluid injection, which initially injects high-temperature fluid for a period of time and then changes to inject low-temperature fluid. The temperature profiles of case A-3 predicted by both analytical solution and COMSOL are illustrated in Figure 9.

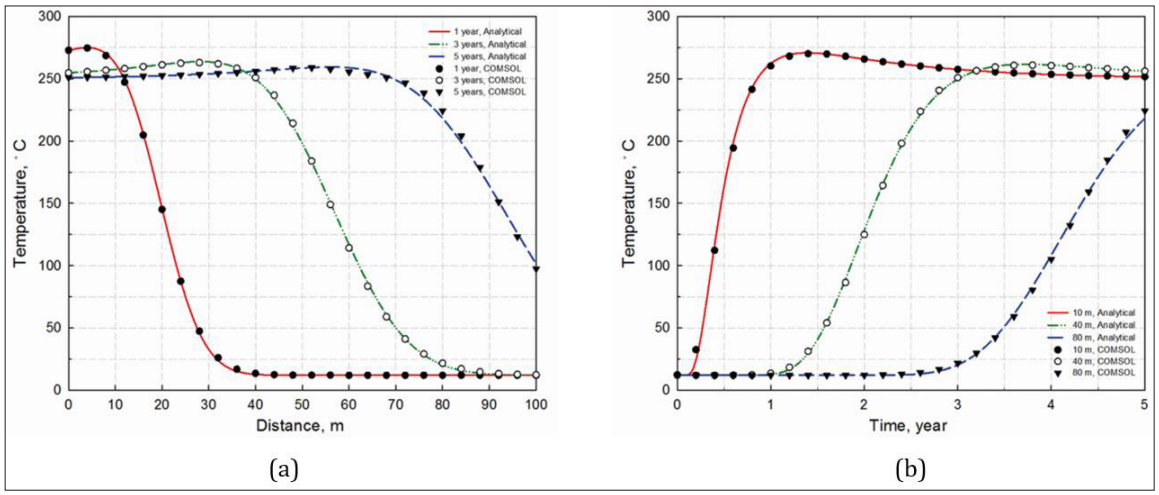

Figure 8: (a) Analytical and numerical temperature distribution as a function of distance from the injection well for case A-2 after 1 year, 3 years, and 5 years of injection; (b) Analytical and numerical temperature propagation as a function of time for case A-2 at the distance of 10 meters, 40 meters, and 80 meters from the injection well.

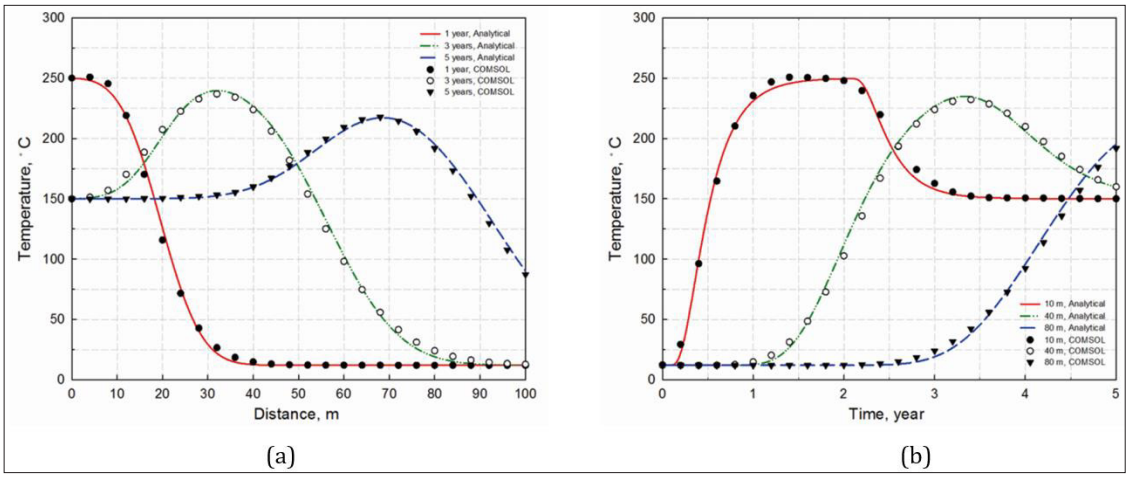

Figure 9: (a) Analytical and numerical temperature distribution as a function of distance from the injection well for case A-3 after 1 year, 3 years, and 5 years of injection; (b) Analytical and numerical temperature propagation as a function of time for case A-3 at the distance of 10 meters, 40 meters, and 80 meters from the injection well.

Case B-1:

a. Mathematical model:

$$\begin{cases} \dfrac{\partial T}{\partial t} = D\dfrac{\partial^2 T}{\partial x^2} - u\dfrac{\partial T}{\partial x} \\ T(x,0) = T_i, \quad x \geq 0 \\ \left(-D\dfrac{\partial T}{\partial x} + uT\right)\Big|_{x=0} = uT_0, \quad t \geq 0 \\ \dfrac{\partial T}{\partial x}\Big|_{x\to\infty} = 0, \quad t \geq 0 \end{cases} \tag{21}$$

b. Analytical solution:

$$T(x,t) = T_i + (T_0 - T_i)\left[\sqrt{\frac{u^2 t}{\pi D}}\, e^{\frac{-(x-ut)^2}{4Dt}} + \frac{1}{2}erfc\left(\frac{x-ut}{2\sqrt{Dt}}\right)\right] - \frac{T_0 - T_i}{2}\left(1 + \frac{ux}{D} + \frac{u^2 t}{D}\right)e^{\frac{ux}{D}}erfc\left(\frac{x+ut}{2\sqrt{Dt}}\right) \tag{22}$$

Case B-1 describes the continuous fluid injection with constant heat flux. The temperature profiles of case B-1 predicted by both analytical solution and COMSOL are illustrated in Figure 10.

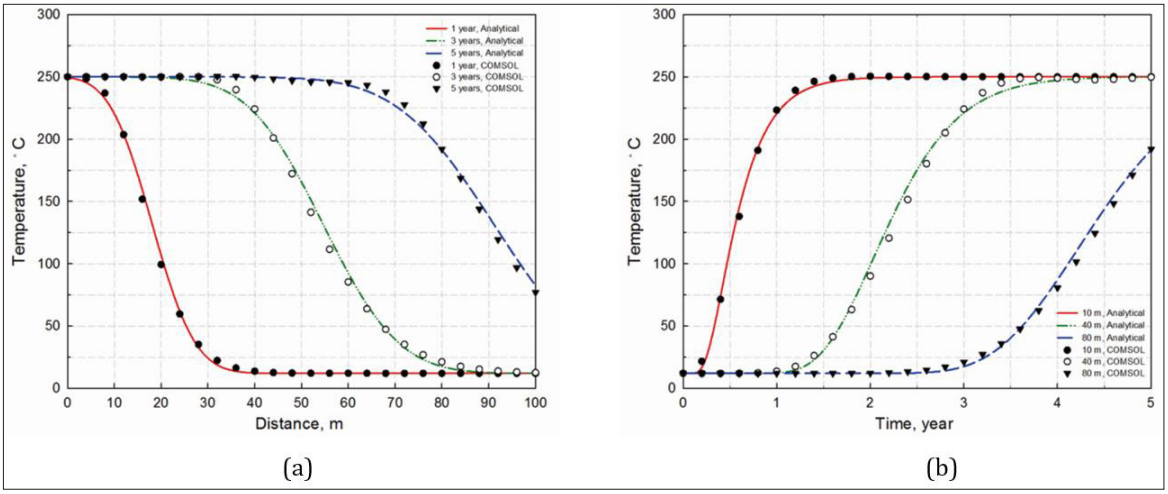

Figure 10: (a) Analytical and numerical temperature distribution as a function of distance from the injection well for case B-1 after 1 year, 3 years, and 5 years of injection; (b) Analytical and numerical temperature propagation as a function of time for case B-1 at the distance of 10 meters, 40 meters, and 80 meters from the injection well.

Case B-2:

a. Mathematical model:

$$\begin{cases} \dfrac{\partial T}{\partial t} = D\dfrac{\partial^2 T}{\partial x^2} - u\dfrac{\partial T}{\partial x} \\ T(x,0) = T_i, \quad x \geq 0 \\ \left(-D\dfrac{\partial T}{\partial x} + uT\right)\Big|_{x=0} = u(T_0 + T_1 e^{-\lambda t}), \quad t \geq 0 \\ \left.\dfrac{\partial T}{\partial x}\right|_{x\to\infty} = 0, \quad t \geq 0 \end{cases} \tag{23}$$

b. Analytical solution:

$$T(x,t) = T_i + (T_0 - T_i)\left[\sqrt{\frac{u^2 t}{\pi D}}\, e^{\frac{-(x-ut)^2}{4Dt}} + \frac{1}{2}erfc\left(\frac{x-ut}{2\sqrt{Dt}}\right)\right] + e^{\frac{ux}{D}}erfc\left(\frac{x+ut}{2\sqrt{Dt}}\right)\left[\frac{u^2 T_1}{2\lambda D} - \frac{T_0 - T_i}{2}\left(1 + \frac{ux}{D} + \frac{u^2 t}{D}\right)\right] + T_1 e^{-\lambda t}\left[\frac{u\, e^{\frac{u-\omega}{2D}x}}{u+\omega}erfc\left(\frac{x-\omega t}{2\sqrt{Dt}}\right) + \frac{u\, e^{\frac{u+\omega}{2D}x}}{u-\omega}erfc\left(\frac{x+\omega t}{2\sqrt{Dt}}\right)\right] \tag{24}$$

where

$$\omega = \sqrt{u^2 - 4\lambda D} \tag{25}$$

Case B-2 describes the continuous fluid injection with exponentially decreasing heat flux. The temperature profiles of case B-2 predicted by both analytical solution and COMSOL are illustrated in Figure 11.

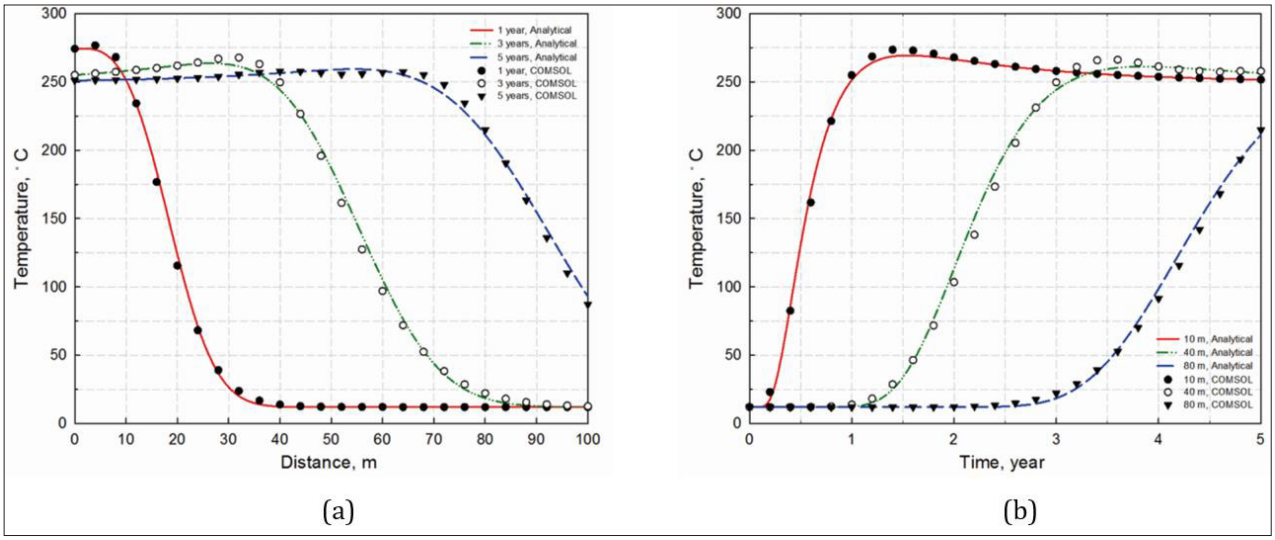

Figure 11: (a) Analytical and numerical temperature distribution as a function of distance from the injection well for case B-2 after 1 year, 3 years, and 5 years of injection; (b) Analytical and numerical temperature propagation as a function of time for case B-2 at the distance of 10 meters, 40 meters, and 80 meters from the injection well.

Case B-3:

a. Mathematical model:

$$\begin{cases} \dfrac{\partial T}{\partial t} = D\dfrac{\partial^2 T}{\partial x^2} - u\dfrac{\partial T}{\partial x} \\ T(x,0) = T_i, \quad x \geq 0 \\ \left(-D\dfrac{\partial T}{\partial x} + uT\right)\Big|_{x=0} = \begin{cases} uT_0, & t \leq t_0 \\ uT_z, & t > t_0 \end{cases} \\ \dfrac{\partial T}{\partial x}\Big|_{x\to\infty} = 0, \quad t \geq 0 \end{cases} \tag{26}$$

b. Analytical solution:

$$T(x,t) = \begin{cases} T_i + (T_0 - T_i)A(x,t), & t \leq t_0 \\ T_i + (T_0 - T_i)A(x,t) + (T_z - T_0)A(x,t-t_0), & t > t_0 \end{cases} \tag{27}$$

where

$$A(x,t) = \sqrt{\frac{u^2 t}{\pi D}}\, e^{\frac{-(x-ut)^2}{4Dt}} + \frac{1}{2}erfc\left(\frac{x-ut}{2\sqrt{Dt}}\right) - \frac{1}{2}\left(1 + \frac{ux}{D} + \frac{u^2 t}{D}\right)e^{\frac{ux}{D}}erfc\left(\frac{x+ut}{2\sqrt{Dt}}\right) \tag{28}$$

Case B-3 describes the periodic fluid injection, which initially injects fluid with high heat flux for a period of time and then changes to inject fluid with low heat flux. The temperature profiles of case B-3 predicted by both analytical solution and COMSOL are illustrated in Figure 12.

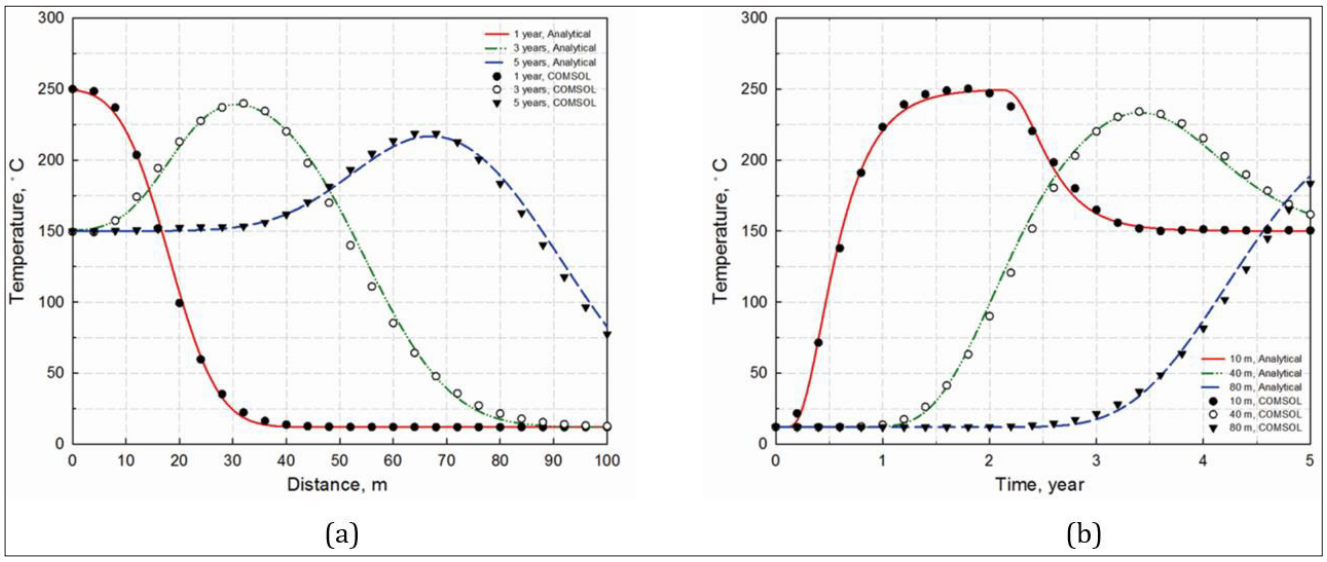

Figure 12: (a) Analytical and numerical temperature distribution as a function of distance from the injection well for case B-3 after 1 year, 3 years, and 5 years of injection; (b) Analytical and numerical temperature propagation as a function of time for case B-3 at the distance of 10 meters, 40 meters, and 80 meters from the injection well.

Case C-1:

a. Mathematical model:

$$\begin{cases} \dfrac{\partial T}{\partial t} = D\dfrac{\partial^2 T}{\partial x^2} - u\dfrac{\partial T}{\partial x} \\ T(x,0) = T_i + T_2 e^{-\beta x}, \quad x \geq 0 \\ T(0,t) = T_0, \quad t \geq 0 \\ \dfrac{\partial T}{\partial x}\Big|_{x\to\infty} = 0, \quad t \geq 0 \end{cases} \tag{29}$$

b. Analytical solution:

$$\begin{aligned} T(x,t) = T_i + \frac{1}{2}(T_0 - T_i)\left[erfc\left(\frac{x-ut}{2\sqrt{Dt}}\right) + e^{\frac{ux}{D}}erfc\left(\frac{x+ut}{2\sqrt{Dt}}\right)\right] \\ + \frac{1}{2}T_2 e^{\beta^2 Dt + \beta ut - \beta x}\left[2 - erfc\left(\frac{x-(u+2\beta D)t}{2\sqrt{Dt}}\right) - e^{\frac{ux}{D}+2\beta x}erfc\left(\frac{x+(u+2\beta D)t}{2\sqrt{Dt}}\right)\right] \end{aligned} \tag{30}$$

Case C-1 describes the continuous fluid injection at constant temperature. The temperature profiles of case C-1 predicted by both analytical solution and COMSOL are illustrated in Figure 13.

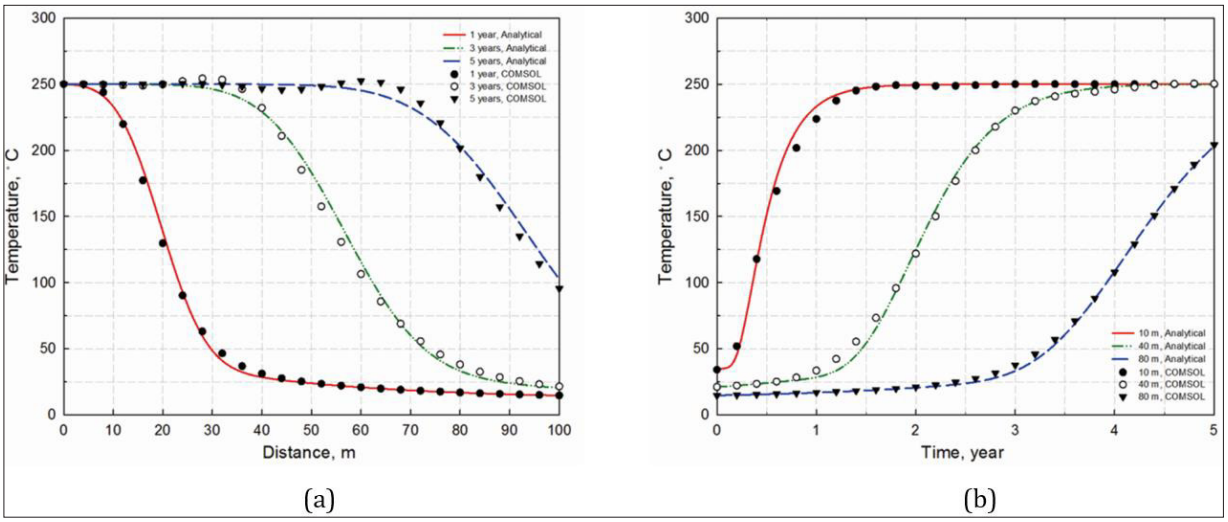

Figure 13: (a) Analytical and numerical temperature distribution as a function of distance from the injection well for case C-1 after 1 year, 3 years, and 5 years of injection; (b) Analytical and numerical temperature propagation as a function of time for case C-1 at the distance of 10 meters, 40 meters, and 80 meters from the injection well.

Case C-2:

a. Mathematical model:

$$\begin{cases} \dfrac{\partial T}{\partial t} = D\dfrac{\partial^2 T}{\partial x^2} - u\dfrac{\partial T}{\partial x} \\ T(x,0) = T_i + T_2 e^{-\beta x}, \quad x \geq 0 \\ T(0,t) = T_0 + T_1 e^{-\lambda t}, \quad t \geq 0 \\ \left.\dfrac{\partial T}{\partial x}\right|_{x\to\infty} = 0, \quad t \geq 0 \end{cases} \tag{31}$$

b. Analytical solution:

$$T(x,t) = T_i + \frac{T_0 - T_i}{2}\left[erfc\left(\frac{x-ut}{2\sqrt{Dt}}\right) + e^{\frac{ux}{D}} erfc\left(\frac{x+ut}{2\sqrt{Dt}}\right)\right] + \frac{1}{2}T_1 e^{-\lambda t}\left[e^{\frac{u-\omega}{2D}x} erfc\left(\frac{x-\omega t}{2\sqrt{Dt}}\right) + e^{\frac{u+\omega}{2D}x} erfc\left(\frac{x+\omega t}{2\sqrt{Dt}}\right)\right] + \frac{1}{2}T_2 e^{\beta^2 Dt + \beta ut - \beta x}\left[2 - erfc\left(\frac{x-(u+2\beta D)t}{2\sqrt{Dt}}\right) - e^{\frac{ux}{D}+2\beta x} erfc\left(\frac{x+(u+2\beta D)t}{2\sqrt{Dt}}\right)\right] \tag{32}$$

where

$$\omega = \sqrt{u^2 - 4\lambda D} \tag{33}$$

Case C-2 describes the continuous fluid injection with exponentially decreasing temperature. The temperature profiles of case C-2 predicted by both analytical solution and COMSOL are illustrated in Figure 14.

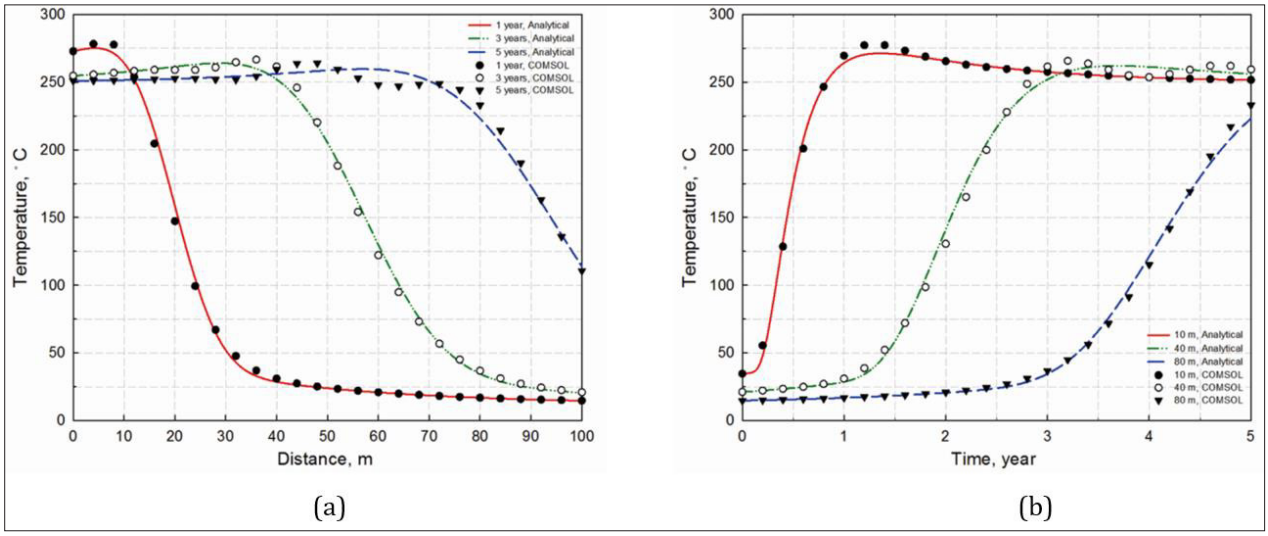

Figure 14: (a) Analytical and numerical temperature distribution as a function of distance from the injection well for case C-2 after 1 year, 3 years, and 5 years of injection; (b) Analytical and numerical temperature propagation as a function of time for case C-2 at the distance of 10 meters, 40 meters, and 80 meters from the injection well.

Case D-1:

a. Mathematical model:

$$\begin{cases} \dfrac{\partial T}{\partial t} = D\dfrac{\partial^2 T}{\partial x^2} - u\dfrac{\partial T}{\partial x} \\ T(x,0) = T_i + T_2 e^{-\beta x}, \quad x \geq 0 \\ \left(-D\dfrac{\partial T}{\partial x} + uT\right)\Big|_{x=0} = uT_0, \quad t \geq 0 \\ \dfrac{\partial T}{\partial x}\Big|_{x\to\infty} = 0, \quad t \geq 0 \end{cases} \tag{34}$$

b. Analytical solution:

$$\begin{aligned} T(x,t) = T_i + (T_0 - T_i)\Bigg[& \sqrt{\frac{u^2 t}{\pi D}} e^{\frac{-(x-ut)^2}{4Dt}} + \frac{1}{2} erfc\left(\frac{x-ut}{2\sqrt{Dt}}\right) - \frac{1}{2}\left(1 + \frac{ux}{D} + \frac{u^2 t}{D}\right) e^{\frac{ux}{D}} erfc\left(\frac{x+ut}{2\sqrt{Dt}}\right)\Bigg] \\ & + \frac{1}{2} T_2 e^{\beta^2 Dt + \beta ut - \beta x}\left[2 - erfc\left(\frac{x-(u+2\beta D)t}{2\sqrt{Dt}}\right)\right] - T_2 \frac{u}{2\beta D} e^{\frac{ux}{D}} erfc\left(\frac{x+ut}{2\sqrt{Dt}}\right) \\ & + \frac{\beta D + u}{2\beta D} T_2 e^{\beta^2 Dt + \beta ut - \beta x} e^{\frac{ux}{D} + 2\beta x} erfc\left(\frac{x+(u+2\beta D)t}{2\sqrt{Dt}}\right) \end{aligned} \tag{35}$$

Case D-1 describes the continuous fluid injection with constant heat flux. The temperature profiles of case D-1 predicted by both analytical solution and COMSOL are illustrated in Figure 15.

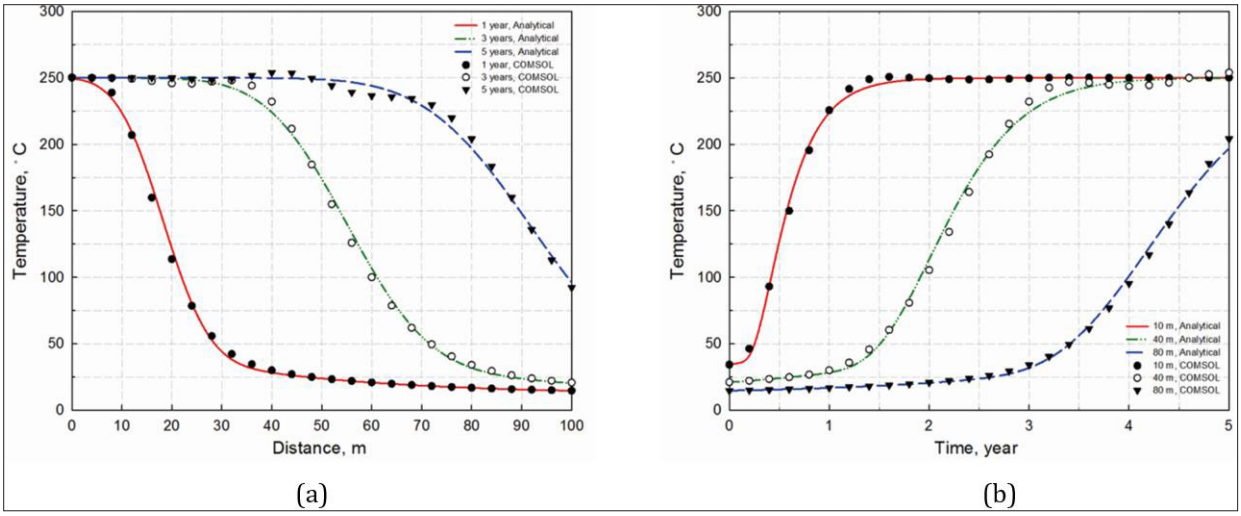

Figure 15: (a) Analytical and numerical temperature distribution as a function of distance from the injection well for case D-1 after 1 year, 3 years, and 5 years of injection; (b) Analytical and numerical temperature propagation as a function of time for case D-1 at the distance of 10 meters, 40 meters, and 80 meters from the injection well.

Case D-2:

a. Mathematical model:

$$\begin{cases} \dfrac{\partial T}{\partial t} = D\dfrac{\partial^2 T}{\partial x^2} - u\dfrac{\partial T}{\partial x} \\ T(x,0) = T_i + T_2 e^{-\beta x}, \quad x \geq 0 \\ \left(-D\dfrac{\partial T}{\partial x} + uT\right)\Big|_{x=0} = u(T_0 + T_1 e^{-\lambda t}), \quad t \geq 0 \\ \dfrac{\partial T}{\partial x}\Big|_{x\to\infty} = 0, \quad t \geq 0 \end{cases} \tag{36}$$

b. Analytical solution:

$$\begin{aligned} T(x,t) = T_i + (T_0 - T_i)\Bigg[& \sqrt{\frac{u^2 t}{\pi D}} e^{\frac{-(x-ut)^2}{4Dt}} + \frac{1}{2} erfc\left(\frac{x-ut}{2\sqrt{Dt}}\right) - \frac{1}{2}\left(1 + \frac{ux}{D} + \frac{u^2 t}{D}\right) e^{\frac{ux}{D}} erfc\left(\frac{x+ut}{2\sqrt{Dt}}\right)\Bigg] \\ & + T_1 e^{-\lambda t}\left[\frac{u}{u+\omega} e^{\frac{u-\omega}{2D}x} erfc\left(\frac{x-\omega t}{2\sqrt{Dt}}\right) + \frac{u}{u-\omega} e^{\frac{u+\omega}{2D}x} erfc\left(\frac{x+\omega t}{2\sqrt{Dt}}\right)\right] + \frac{u^2}{2\lambda D} T_1 e^{\frac{ux}{D}} erfc\left(\frac{x+ut}{2\sqrt{Dt}}\right) \\ & - \frac{u}{2\beta D} T_2 e^{\frac{ux}{D}} erfc\left(\frac{x+ut}{2\sqrt{Dt}}\right) + T_2 e^{\beta^2 Dt + \beta ut - \beta x}\left[1 - \frac{1}{2} erfc\left(\frac{x-(u+2\beta D)t}{2\sqrt{Dt}}\right)\right] \\ & + \frac{\beta D + u}{2\beta D} T_2 e^{\beta^2 Dt + \beta ut + \beta x + \frac{ux}{D}} erfc\left(\frac{x+(u+2\beta D)t}{2\sqrt{Dt}}\right) \end{aligned} \tag{37}$$

where

$$\omega = \sqrt{u^2 - 4\lambda D} \tag{38}$$

Case D-2 describes the continuous fluid injection with exponentially decreasing heat flux. The temperature profiles of case D-2 predicted by both analytical solution and COMSOL are illustrated in Figure 16.

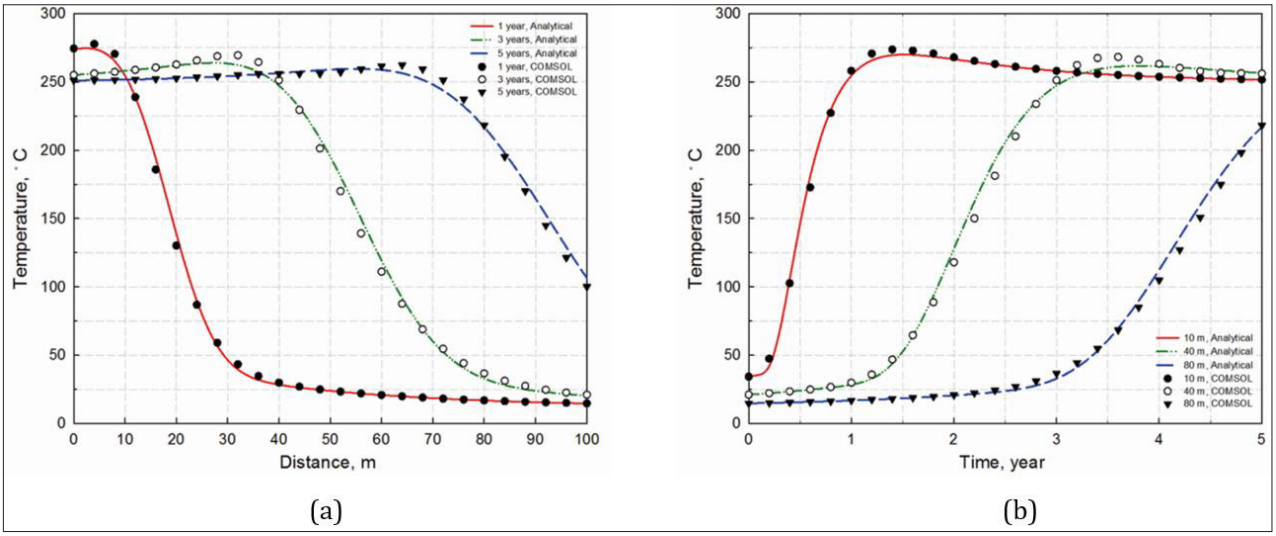

Figure 16: (a) Analytical and numerical temperature distribution as a function of distance from the injection well for case D-2 after 1 year, 3 years, and 5 years of injection; (b) Analytical and numerical temperature propagation as a function of time for case D-2 at the distance of 10 meters, 40 meters, and 80 meters from the injection well.

Results and Discussion

Efficiency of heat convection

The analytical solution of pure conduction [15] and the analytical solution of case A-1 are used in the comparison, and the temperature curves are displayed in Figure 17. It is found that heat convection plays a significant role in accelerating heat transfer. The rate of convective heat transfer is much faster than the rate of conductive heat transfer, and convection accounts for a much higher percentage of the total heat transferred than conduction.

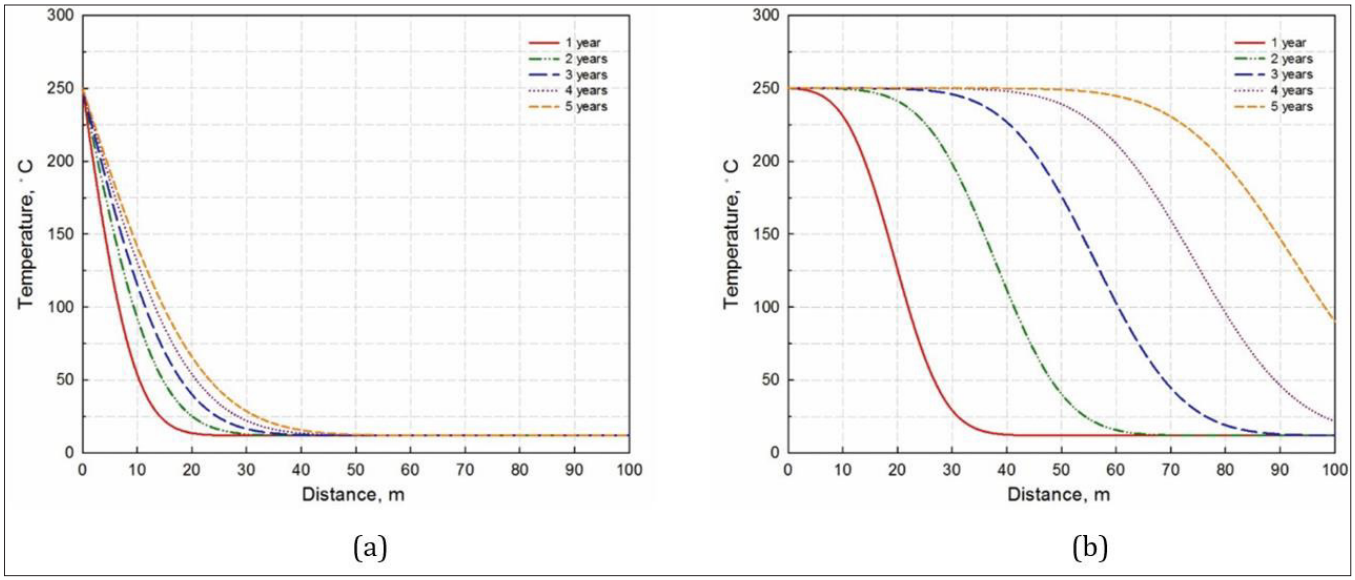

Figure 17: (a) Analytical temperature distribution as a function of distance from the injection well for pure conduction; (b) Analytical temperature distribution as a function of distance from the injection well for the combination of convection and conduction.

Analytical solution

In each case study, a unique heat transfer model coupled with steady flow is developed. The new heat transfer models are constructed by one-dimensional convection-diffusion equation with different initial and boundary conditions. Heat convection and heat conduction are integrated in these models. Analytical solutions to these new heat transfer models are developed successfully. The temperature curves of the analytical solutions are displayed in Figure 7 to Figure 16.

Numerical simulation

COMSOL simulation: All the heat transfer processes in the cases studies can be numerically simulated using COMSOL. The temperature curves predicted by COMSOL are also plotted in Figure 7 to Figure 16, so as to easily conduct the comparison with the results of analytical solutions. It is found that the temperature curves of analytical solutions show excellent consistence with the results of COMSOL simulations. The temperature curves of analytical solutions are much smoother than the results of COMSOL simulations, which reflects the instability of numerical simulation caused by the numerical dispersion of the finite element method used in COMSOL.

CMG simulation: The temperature profiles of the middle layer in x-direction of SAGD simulation model are exported from CMG in order to conduct the comparison with the results of case A-1. The temperature curves predicted by the analytical solution of case A-1 and the SAGD simulation are plotted in Figure 18. It is found that there exist reasonable agreements between the temperature curves predicted by the analytical solution in this study and those predicted by CMG simulation. However, CMG simulation is complex and time-consuming compared to the simple mathematical model in this study.

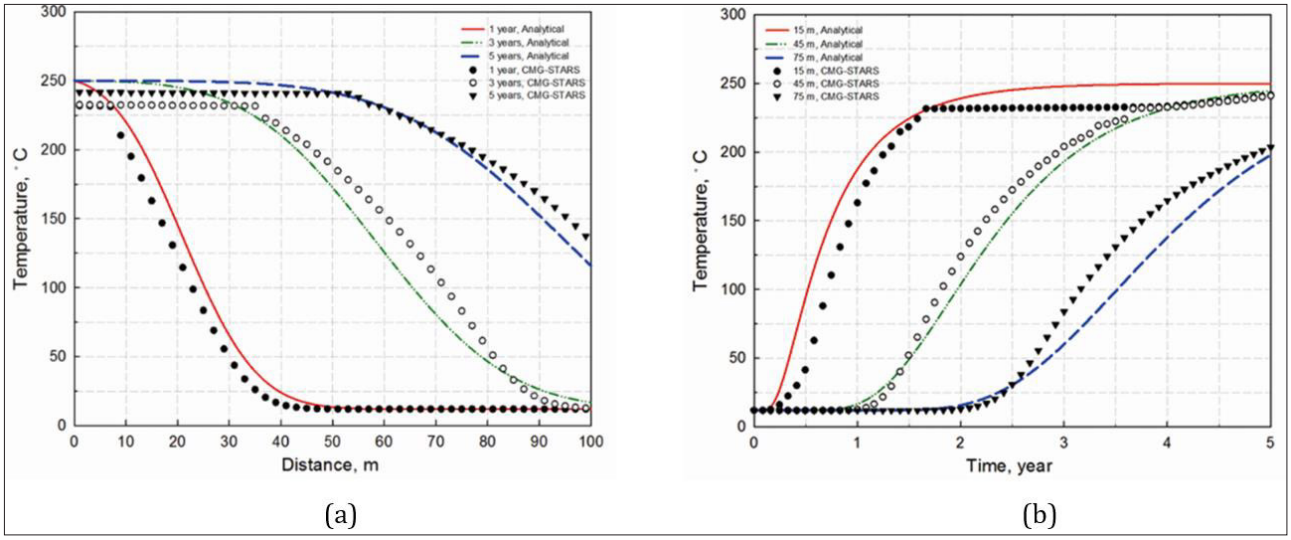

Figure 18: (a) Analytical and CMG temperature distribution as a function of distance from the injection well after 1 year, 3 years, and 5 years of injection; (b) Analytical and CMG temperature propagation as a function of time at the distance of 15 meters, 45 meters, and 75 meters from the injection well.

Sensitivity analysis

Thermal diffusivity measures the ability of a subsurface reservoir to conduct thermal energy, which indicates how quick a subsurface reservoir reacts to a change in surrounding temperature. Thermal convection velocity measures the ability of the injection fluid to transport its heat energy along the direction of the fluid flow, which describes how fast the hot fluid can transport its heat energy to further distances [11]. The sensitivity analysis of base case A-1 is performed to study the effects of thermal diffusivity and thermal convection velocity on heat transfer.

Effect of thermal diffusivity: In Figure 19(a), it is found that for a subsurface reservoir and fluid system with larger thermal diffusivity, the heating area is larger, and the slope of temperature curve is smaller, which means temperature gradient is smaller. This is because a subsurface reservoir and fluid system with large thermal diffusivity can conduct heat quickly and adjust its temperature to that of their surroundings more rapidly. In Figure 19(b), the results indicate that for a subsurface reservoir and fluid system with larger thermal diffusivity, reservoir temperature begins to increase earlier at the same observation location, but the increasing rate of subsurface reservoir temperature is smaller at the same observation location. This is because a subsurface reservoir with large thermal diffusivity has poor ability to store thermal energy [12-15].

Figure 19(a) and (b) show that there always exists a cross point at a certain location or time. The cross point in Figure 19(a) represents location of the middle point in transition zone, i.e., steam and oil mixing zone. The temperature of the middle point in transition zone is always constant. When the thermal convection velocities are the same, the middle points of transient zone are crossed at the same location after three years, which indicates that the location of this middle point is determined by thermal convection velocity. The cross point in Figure 19(b) represents the time needed for the middle point in transition zone travels to the specific location x=40 meter. When the thermal convection velocities are the same, the middle points in transient zone are crossed after same time period. In Figure 19(a) and(b), the temperatures of the two cross points are almost the same, which proves that the crossed point is just the middle point of the transition zone. The location of the cross point is determined by thermal convection velocity, and thermal diffusivity only affects the temperature distribution around the middle point in transition zone.

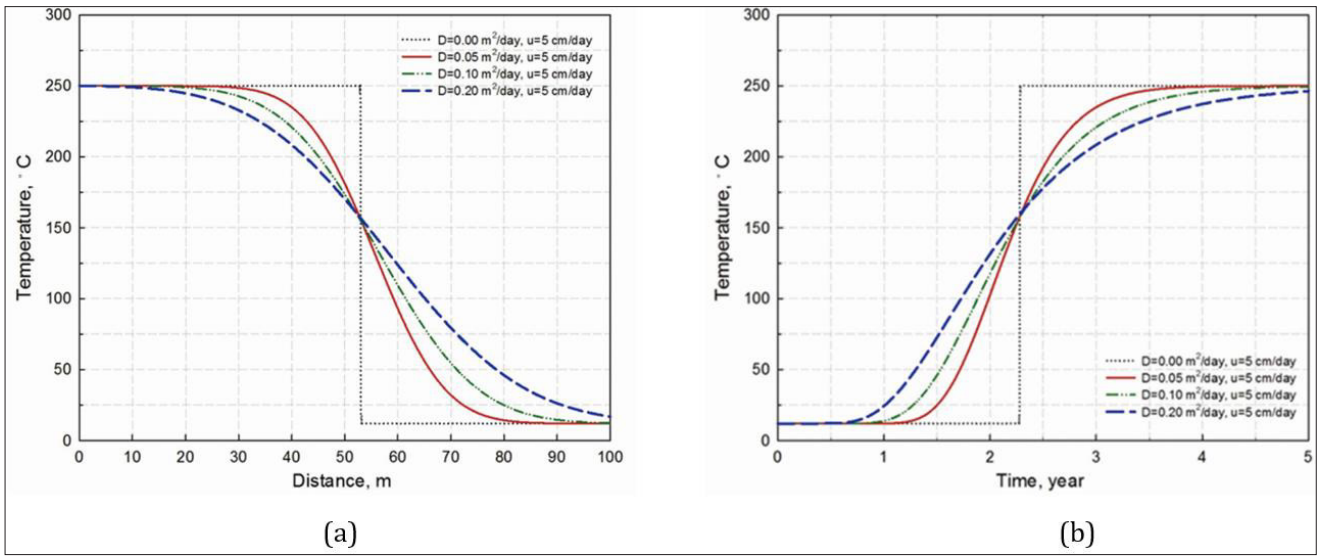

Figure 19: (a) Analytical temperature distribution as a function of distance from the injection well for case A-1 with different thermal diffusivities after 3 years of injection; (b) Analytical temperature propagation as a function of time for case A-1 with different thermal diffusivities at the distance of 40 meters from the injection well.

Effect of thermal convection velocity: In Figure 20(a), it is found that when fluid is injected at a higher thermal convection velocity, heat can be transported to further distance after three years. The slopes of the temperature curves are nearly the same with different thermal convection velocities, which is because the thermal diffusivities are the same. In Figure 20(b), the results indicate that when fluid is injected at a higher thermal convection velocity, the subsurface reservoir temperature begins to increase earlier at the same observation location, and the increasing rate of subsurface reservoir temperature is larger at the same observation location. This is because fluid injection at high thermal convection velocity can accelerate the convective heat transfer.

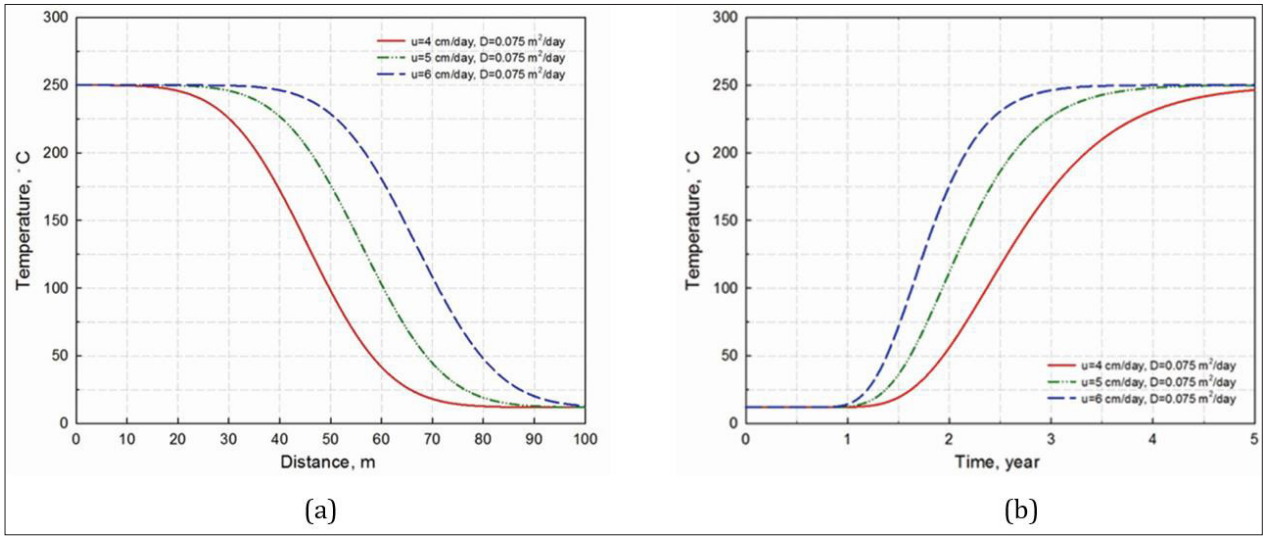

Figure 20: (a) Analytical temperature distribution as a function of distance from the injection well for case A-1 with different thermal convection velocities after 3 years of injection; (b) Analytical temperature propagation as a function of time for case A-1 with different thermal convection velocities at the distance of 40 meters from the injection well.

Conclusion

This study proposed novel mathematical models integrating heat conduction and heat convection to describe transient heat transfer coupled with steady flow in thermal recovery and geothermal reservoir production process. The following conclusions are drawn from this work:

- Convective and conductive heat transfer occur simultaneously during thermal recovery process. Heat convection plays a significant role in accelerating heat transfer. Fluid flow motivates convective heat transfer and greatly increases the rate of heat

transfer. Heat convection accounts for a much higher percentage of the total heat transferred than heat conduction.

- The temperature curves of analytical solutions in this study are reasonably consistent with the numerical simulation results obtained by running COMSOL and CMG simulation. In the subsurface reservoir and fluid system with larger thermal diffusivity, the heating area is larger and the temperature increasing rate is smaller at the same observation location. When the fluid is injected at a higher thermal convection velocity, heat can be transported to further distance, and the temperature increasing rate is larger at the same observation location.
- The newly proposed mathematical models and newly developed analytical solutions are simple and efficient for temperature transient analysis. They are very useful to quickly obtain the temperature curves in thermal recovery process. The further extension of these solutions to more complicated cases will be studied in future research for subsurface thermal heavy oil and geothermal fluid production processes.

Acknowledgment

The authors would like to acknowledge the partial financial support from the Petroleum Technology Research Centre (PTRC) in the form of innovation fund is greatly appreciated by the authors. Our thanks also go to Computer Modelling Group and COMSOL for providing the licenses of numerical simulators.

Conflict of interests

The authors declare that they have no known competing financial interests or personal relationships that could have appeared to influence the work reported in this paper.

References

1. AEUB, ST98-2007 (2007) Alberta's Energy Reserves 2006 and Supply/Demand Outlook 2007-2016. ISSN 1910-4235, Farhood Rahnama, Coordinator, Alberta Energy and Utilities Board, Calgary, Alberta, Canada.
2. ERCB, ST98-2011 (2011) Alberta's Energy Reserves 2010 and Supply/Demand Outlook 2011-2020. ISSN 1910-4235, Carol Crowfoot, Coordinator, Energy Resources Conservation Board, Calgary, Alberta, Canada.
3. MA Wilson, RW Bennett (1985) Evaluation of Saskatchewan's Heavy Oil Reserves, Saskatchewan Energy and Resources, Saskatchewan, Canada.
4. SM Farouq Ali (2003) Heavy oil - Ever more mobile. J Petrol Sci Eng 37: 5.
5. RM Butler, GS McNab, HY Lo (1981) Theoretical studies on the gravity drainage of heavy oil during in-situ steam heating. Can J Chem Eng 59: 455.
6. E Vittoratos, GR Scott (1990) Cold Lake Cyclic Steam Stimulation: A Multiwell Process. C.I Beattie, SPE Res Eng 5: 19-24.
7. RG Moore, CJ Laureshen, JDM Belgrave, MG Ursenbach, SA Mehta (1995) In Situ Combustion in Canadian Heavy Oil Reservoirs. Fuel 74: 1169.
8. H Alboudwarej, J Felix, S Taylor, R Badry, C Bremner, et al. (2006) Highlighting Heavy Oil. Oilfield Review 18: 34.
9. RM Butler (1991) Thermal Recovery of Oil and Bitumen. Prentice Hall, Englewood Cliffs, New Jersey p. 31-37.
10. K Yu (2014) Analytical Modeling of Transient Heat Transfer Coupled with Fluid Flow in Heavy Oil Reservoirs during Thermal Recovery Processes, Master thesis. University of Regina, Regina, Canada, pp. 8-22.
11. K Yu, G Zhao (2016) Modeling of Heat Transfer Coupled with Fluid Flow for Temperature Transient Analysis during SAGD Process. SPE Latin America and Caribbean Heavy and Extra Heavy Oil Conference, Society of Petroleum Engineers, Lima.
12. M Irani, S Ghannadi (2013) Understanding the Heat-Transfer Mechanism in the Steam-Assisted Gravity-Drainage (SAGD) Process and Comparing the Conduction and Convection Flux in Bitumen Reservoirs. SPE J 18: 134-145.
13. DP Baston (2008) Analytical and Numerical Modeling of Thermal Conductive Heating in Fractured Rock. Master thesis, Queen's University, Kingston, Canada, pp. 7-9.
14. M Th van Genuchten, WJ Alves (1982) Analytical Solutions of One-Dimensional Convective-Dispersive Solute Transport Equation. Technical Bulletin Number 1661. U.S. Department of Agriculture, Washington, USA, pp. 3-4.
15. HS Carslaw, JC Jaeger (1959) Conduction of Heat in Solids, 2nd edition. Oxford University Press, Landon, pp. 58-70.